Mathematical Biosciences 284 (2017) 3–11

Contents lists available at ScienceDirect

Mathematical Biosciences

journal homepage: www.elsevier.com/locate/mbs

A new data-driven model for post-transplant antibody dynamics in high risk kidney transplantation

Yan Zhang[a], David Briggs[b], David Lowe[b,c,d], Daniel Mitchell[d], Sunil Daga[d,e], Nithya Krishnan[e], Robert Higgins[e], Natasha Khovanova[a,*]

[a] School of Engineering, University of Warwick, UK
[b] NHS Blood and Transplant, Birmingham, UK
[c] Department of Histocompatibility and Immunogenetics, Royal Liverpool University Hospital, Liverpool, UK
[d] Clinical Sciences Research Laboratories, University of Warwick, Coventry, UK
[e] Renal Unit, University Hospitals Coventry and Warwickshire, Coventry, UK

ARTICLE INFO

Article history:
Available online 14 May 2016

Keywords:
Kidney transplantation
Antibody dynamics
Ordinary differential equations
Data driven model
Eigenvalue
Variational Bayesian inference

ABSTRACT

The dynamics of donor specific human leukocyte antigen antibodies during early stage after kidney transplantation are of great clinical interest as these antibodies are considered to be associated with short and long term clinical outcomes. The limited number of antibody time series and their diverse patterns have made the task of modelling difficult. Focusing on one typical post-transplant dynamic pattern with rapid falls and stable settling levels, a novel data-driven model has been developed for the first time. A variational Bayesian inference method has been applied to select the best model and learn its parameters for 39 time series from two groups of graft recipients, i.e. patients with and without acute antibody-mediated rejection (AMR) episodes. Linear and nonlinear dynamic models of different order were attempted to fit the time series, and the third order linear model provided the best description of the common features in both groups. Both deterministic and stochastic parameters are found to be significantly different in the AMR and no-AMR groups showing that the time series in the AMR group have significantly higher frequency of oscillations and faster dissipation rates. This research may potentially lead to better understanding of the immunological mechanisms involved in kidney transplantation.

1. Introduction

Kidney transplantation is proven to be the best treatment for renal failure and success is dependent on the reaction of the immune system primarily against human leukocyte antigen (HLA) proteins of the transplant. The HLA system is extremely complex; it is unusual to find two unrelated individuals with the same HLA type and only a minority of the transplants in the UK are *fully matched* for HLA tissue proteins [1]. Conventional transplantation is facilitated by immunosuppression which targets cellular components of the immune system.

A significant number of patients develop antibodies to HLA following exposure to non-self HLA from pregnancy, blood transfusion or previous kidney graft [2,3]. These antibodies exist as multiple isoforms but it is Immunoglobulin G (IgG) which is deemed to be most detrimental to transplant outcome [4]. Such IgG, termed donor-specific antibody (DSA), when directed at a current or prospective donor HLA, can persist for years and are a barrier to transplantation because they can cause immediate, early, and late rejection. Safe transplantation of potential recipients with high levels of circulating DSAs is an ongoing problem resulting in prolonged waiting times for transplantation [5]. Ideally, such recipients should receive a transplant from an antibody compatible donor but because of a donor shortage this is seldom possible.

Innovative clinical protocols and techniques have been developed [5–7] to allow transplantation of such highly sensitised patients by removal of DSAs immediately before the transplant [2,8]. Complete elimination of preformed HLA DSAs is not possible and, because of immunological memory, post-transplant DSA resynthesis can still result in severe acute antibody-mediated rejection (AMR) and an increased risk of graft loss. The mechanisms underlying the control of antibody production are poorly understood and treatments given to patients with AMR can be ineffective. In recent years, a number of publications [9–11] have confirmed that HLA antibodies are the major cause of acute AMR and chronic graft

* Corresponding author. Tel.: +44 2476528242.
E-mail address: n.khovanova@warwick.ac.uk (N. Khovanova).

http://dx.doi.org/10.1016/j.mbs.2016.04.008

failure. Even though the risk of acute rejection and chronic graft failure is positively correlated with high DSA levels, the association can vary between patients. In the acute setting, transplantation across very high DSA levels may result in 50% graft loss, but data based on the currently used antibody detection assays cannot reliably predict the outcome [12]. Likewise, in the chronic setting there is not always a clear relationship between the occurrence of AMR and the detection of circulating DSAs [13,14].

Our group has investigated early DSA dynamics in these high risk transplants because the nature of their response is likely to profoundly affect clinical outcomes [2,8,15]. We have observed that the dynamic behaviour of post-transplant DSAs varies from case to case, and even different DSAs in the same patient (targeting different HLA) show diverse patterns. Development of a strong mathematical approach to describe the dynamics of the preformed DSAs has not yet been attempted. This is because white box models, i.e. physiological models, are not yet feasible due to the complexity of underlying immunological responses to transplants. Data-driven models, on the other hand, require both an accurate method of measuring the DSAs in human sera and an appropriate mathematical framework for the development of the model from limited and complex sets of data.

The possible mechanisms underlying changes in the levels of DSAs are complex and the DSAs levels cannot easily be measured in the laboratory. DSA levels may change because of rises and falls in the rate of production. This itself could be related to changes in the populations of antibody-producing cells (plasma cells and memory B lymphocytes), and these cells could be formed pre-transplant and/or recruited from less mature lymphocyte populations post-transplant [16]. Falls in the levels of DSA post-transplant are very interesting, as these may occur much faster than the 'natural' rate of antibody clearance from the body (thought to have a half life of about 20–30 days [17]). Mechanisms associated with reductions in antibody levels could include absorption of antibodies onto HLA molecules on the graft [18] – it is known that the levels of HLA on a graft may increase post-transplant, but this cannot yet be quantified. Some HLA is shed by the graft, so antibodies could be absorbed in the circulation. It is known that one physiological method used by the body to control antibody levels is to produce antibodies that block other antibodies (idiotypic antibodies), and production of idiotypic antibodies could explain the falls in DSA post-transplant [19]. However, as with other potential regulatory mechanisms, it is currently hard to measure idiotypic antibodies accurately. Thus, mathematical modelling of changes in DSA levels may indicate where the efforts involved in developing new laboratory assays might be best directed, and once appropriate assays are available, the modelling may help in the interpretation of results of the assays at different time points. This could be particularly important in relation to falls in DSA levels, since this is a key clinical objective that is currently not achievable in clinical practice.

It has recently been recognised by the transplant community [2,20] that post-transplant screening for anti-HLA antibodies could be an important tool for monitoring of transplant recipients. Highly sensitive and specific assays using purified HLA protein have been developed in recent years. This development in assays meets the increasing need for monitoring post-transplant DSAs [21] and opens up opportunities to develop data-driven mathematical models for the evolution of antibodies after transplantation.

A unique dataset with detailed antibody measurements spanning three to six months, starting around ten days before transplantation has been obtained by our group. A previous analysis [2] of these data revealed various patterns of antibody dynamics, both with or without acute AMR. Some DSA time series show a rapid rise during the first two weeks followed by a rapid fall to almost undetectable levels, which then remain low. This finding is striking: in many of these patients, the DSAs had persisted for many years before transplantation, and therapies used experimentally have been unable to stop antibody production before transplantation. A better understanding of this phenomenon could therefore have practical benefits.

The aim of this work is therefore to describe the pathological early antibody response in mathematical terms and we hypothesize that this approach might enable a more intelligent application of laboratory testing and suggest therapeutic approaches to selectively control this antibody response and improve clinical transplant outcomes. To take full advantage of the data available, we have developed a data-driven model based on differential equations that reflects the continuous nature of the underlying immunological process [22]. The usefulness of the model for classification between patients with and without AMR was also investigated.

Data from the patients in this series were analysed in relation to a single outcome measure, namely the occurrence of early acute AMR. This is a key early outcome in antibody incompatible transplantation (AIT), as it is associated with the levels of immunosuppression required in the early post-transplant period, and is also associated with short and long term graft survival.

The structure of the paper is as follows. Section 2 gives details on the data and presents visual analysis of the variety of dynamic antibody responses to transplantation. Section 3 explains the methodology for model formulation and parameter estimation. Section 4 presents the final model and detailed analysis of systems parameters. Section 5 summarises the results, justifies the need for further work and outlines the relevance of the model for kidney transplant management.

2. Data description and visual analysis of dynamic patterns

Data from twenty-three patients who underwent renal AIT at University Hospitals Coventry and Warwickshire (UK) between 2003 and 2012 were analysed in this study. The data were comprised of time series of DSA evolution over a period of about ten days before and six months after transplantation. Serum samples for DSA analysis were taken almost daily in the first three to four weeks, as most dynamic behaviour occurs during that period, and sampling became more sparse later when the antibodies tended to be more stable. Antibody levels were measured using the microbead assay manufactured by One Lambda Inc (Canoga Park, CA, USA), analysed on the Luminex platform (XMap 200, Austin, TX, USA). The assay measures the Mean Fluorescence Intensity (MFI) which corresponds to antibody level although their relationship is linear only over a limited range. As described in [2], when the MFI value is higher than 10,000 AU (Arbitrary Units) and below about 1000 AU, the linear correlation breaks.

Some of the patients had multiple DSAs targeting different HLA, so the total number of post-transplant time series available for this analysis was *thirty-nine. Twenty-seven DSA time series* belong to fourteen patients that experienced episodes of acute AMR in the first thirty days after transplantation (AMR group), and *twelve DSA time series* belong to the other nine patients who did not have an episode of AMR (no-AMR group). Rejection episodes were diagnosed by renal biopsy or clinically if there was rapid onset of oliguria with a rise in both serum creatinine and DSA levels [2]. In patients receiving HLA antibody-incompatible grafts, the incidence of AMR was 30–40% [15]. Although AMR can be severe and can eventually result in graft failure, it usually develops slowly over a period of several days. This gives an opportunity to detect AMR at an early stage and treat it, resulting in better outcomes [8]. The group characteristics and details of therapy have previously been described [2]. A smaller dataset including *twenty-one* time series from the first twelve patients in the cohort was considered in our preliminary study [23].

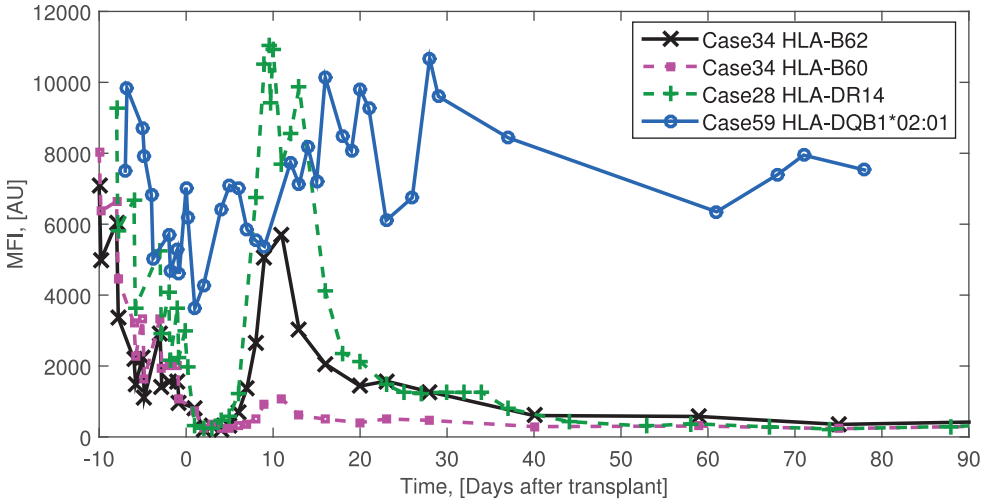

Fig. 1. Measured time series illustrating individual DSA changes in the no-AMR group. Markers correspond to each measurement point. MFI = mean fluorescent intensity.

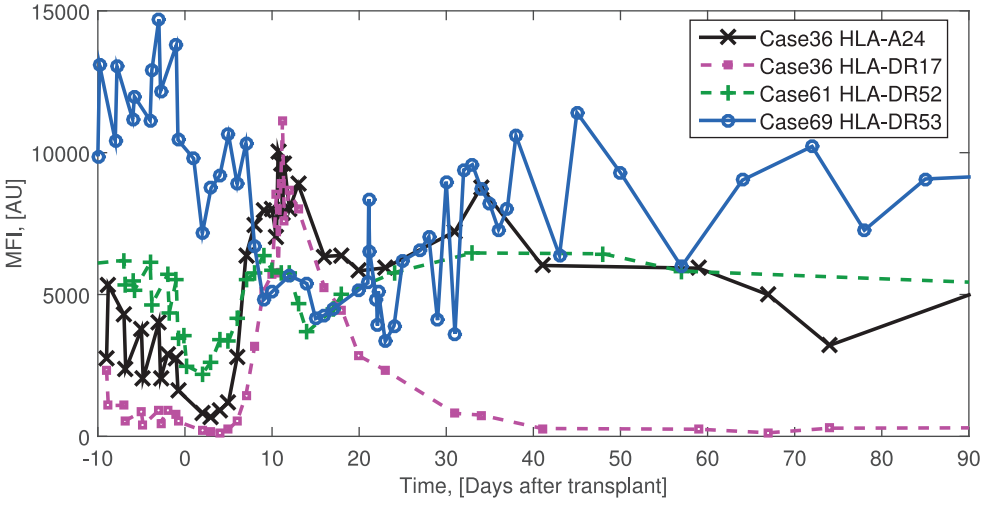

Fig. 2. Measured time series illustrating individual DSA changes in the AMR group. Markers correspond to each measurement point. MFI = mean fluorescence intensity.

Visual examination of the time series reveals diverse dynamic behaviour of DSAs. Figs. 1 and 2 show some examples of the patterns from the no-AMR group and the AMR group, respectively. As some patients had multiple DSAs, the case number in these figures and in the corresponding text is followed by the DSA type. For example, in Fig. 2, patient 36 had two DSAs, HLA-A24 and HLA-DR17, comprising two different time series: case 36 HLA-A24 (case 36 A24 for short) and case36 HLA-DR17 (case 36 DR17 for short). Pretransplant antibody removal can be seen to reduce total DSA levels due to cycles of double filtration plasmapheresis. Typically, between two and five alternate day sessions were performed.

The initial drop is typically followed by a rapid rise in DSA which usually occurs with a lag of a few days after transplantation and is caused by two factors: plasmapheresis stopping and an increased rate of DSA synthesis due to an immunological memory response. After the peak levels a diversity of dynamic patterns is noticeable: antibody levels do not follow a common route, varying from case to case, and even differing for different DSAs in the same patient. In some cases there is a rapid fall in DSA to a steady state, corresponding to a low (almost zero) level of DSA, and this is typically reached within the first month after operation. Such patterns are observed in both no-AMR and AMR groups: case 34 (both B62 and B60) and case 28 in Fig. 1, and case 36 DR 17 in Fig. 2. In other cases the dynamics of the fall after the peak are followed by another rise, and antibodies do not settle at a low level within the first three months after operation: case 59 in Fig. 1, case 36 A24 and cases 61 and 69 in Fig. 2. They either demonstrate a slow dynamic around a certain constant level (case 61 in Fig. 2) or change dramatically over the first three months (case 59 in Fig. 1 and case 69 in Fig. 2). There is no obvious relationship between these dynamical patterns, steady state levels and the occurrence of AMR episodes. In some cases, as shown above, low steady state levels are observed in the no-AMR group and higher levels or dramatic changes are noticeable in the AMR group. There are also cases with the absence of AMR despite high levels of DSA, or presence of AMR despite low DSA levels. Finally, some patients (e.g. case 36 in Fig. 2) rejected the kidney, but had multiple DSAs with one type that rose after the initial fall post-transplant (A24) and another type that kept falling to a low steady level (DR17). This visual analysis demonstrates that there is no certain association between higher levels of post-transplant DSA and the occurrence of the rejection episodes.

The aim of this study is to analyse these dynamical patterns in order to propose a set of characteristics capable of discriminating

between the patients with and without the incidence of AMR. In this study, we are particularly interested in the DSA dynamics after the first peak value down to an almost zero level, i.e. focus is on the typical pattern of a rapid fall that occurs in most of the patients with and without AMR episodes. Falls in the serum levels of HLA DSAs after kidney transplantation are of great clinical interest, as they are associated with resolution of rejection and good long term outcomes in patients at high risk of graft loss [15].

3. Models and methods

3.1. Data fitting and model selection

As seen from the preliminary observations of the dynamic patterns, the HLA antibody response to the transplanted kidney is a complex immunological process, nonlinear and stochastic in general. Time series available for analysis are complex and one-dimensional: only one variable as a function of time (MFI levels) is available representing a response of the entire biological system to external stimuli. These characteristics pose a set of challenging questions with respect to the order of the system and the number of parameters to be used in the model. It is also unclear whether the system equation should be linear or nonlinear, stochastic or deterministic, and what would be the most appropriate modelling approach to identify system parameters in the situation where no preliminary knowledge of the model is available. Although we only consider the falling part of MFI level dynamics, all the above questions remain.

3.1.1. Exponential fitting

It can be noticed that the falling MFI dynamics of HLA DSA after the peak value is a relaxation process, the simplest theoretical description of which is an exponential law. Initially the curve fitting tool (Cftool) in Matlab [24] was used to fit each of the thirty-nine DSAs. Some of the time series were correctly described by this approach; however, the use of superposition of exponential functions could not correctly describe all the cases with and without AMR in our cohort. As the next step, instead of exponential functions, i.e. *solutions* of dynamic equations, dynamic mathematical models in the form of differential equations were considered.

3.1.2. Form of the model: linear/nonlinear and stochastic terms

A general form of an nth order nonlinear differential equation with coefficients in the form of a polynomial function have been considered. Initially two stochastic terms were included to represent noise in the system equations. Measurement noise is added due to uncertainty in measured data, and the dynamic noise accounts for any other hidden properties not captured by the model. Thus, DSA falls after the initial rise (to a peak level) in the early post-transplant period can be described by the following model:

$$\frac{\mathrm{d}^n}{\mathrm{d}t^n}x_t + \sum_{i=0}^{n-1} f_{i+1}(x_t)\frac{\mathrm{d}^i}{\mathrm{d}t^i}x_t + f_0(x_t) = \eta_t \tag{1}$$

$$y_t = x_t + \varepsilon_t \tag{2}$$

Eq. (1) is an evolution equation of nth order, where x_t is a function of t that describes the MFI dynamics, and y_t is the measured MFI time series. η_t is system noise, and ε_t is measurement noise. Each noise was modelled as Gaussian-distributed white noise with zero mean and intensity (variance) of I_η and I_ε, respectively. $f_{i+1}(x_t)$ $(i = 0, 1, \ldots, n-1)$ are polynomial functions of x_t. The derivative of order zero of x_t is defined to be x_t itself. $f_0(x_t)$ is defined as $-\theta_0$ for convenience. The order of the system equation n is to be decided together with unknown parameters of functions $f_{i+1}(x_t)$. n initial conditions are required to obtain a closed form solution.

Model M_n constituting Eqs. (1) and (2) covers a variety of dynamic patterns depending on the order of the system n. A more complex model may be able to explain a wider range of system behaviour in the data at the risk of overfitting.

3.2. Model and parameter identification

In the current work, for DSA time series, nonlinear and linear stochastic dynamic hierarchical models were developed using a variational Bayesian inference approach [25] for both model and parameter identification. Both the form and parameters of the models were identified using the SPM9 toolbox [26] (freely available online) for MATLAB [24]. This variational Bayesian toolbox [26] allows accounting for both types of stochastic terms: measurement noise and system noise.

Starting from the first order model M_1 ($n = 1$ in Eq. (1)), the order n was increased until the model M_n fitted the data sufficiently well – satisfy the criteria given in Section 3.3. The variational Bayesian learning algorithm [25] was modified to our specific data to calculate probabilities $p(y_t|M)$ (where M is M_1, M_2, ..., M_n) of observing the time series y_t given different models M, so that the model with the highest value of $p(y_t|M)$ could be selected for that specific DSA time series. Attention has to be paid to the features in the dataset that can be explained by a model with a higher order but cannot be explained by the model with a lower order, and to decide if the features are general enough to make the final decision on the order for all DSA time series under investigation.

For each model candidate, the value of the probability $p(y_t|M)$, which is also referred to as the model evidence [27], was approached by iteratively optimising the states of the system and model parameters until a local maximum value of $p(y_t|M)$ was reached. This procedure is embedded into the variation Bayesian optimisation algorithm [27]. Briefly, to infer multiple elements of the hierarchical model, i.e. system states, parameters (related to the deterministic terms in the equation), and hyperparameters (related to the stochastic terms) each element is optimised one by one while the rest of the elements are kept fixed. There are two steps in this optimisation procedure. Firstly, assuming the elements (parameters and the states) are conditionally independent of each other, the combined distribution can be factorised into independent partitions of each element distribution, which is known as the mean-field approximation, i.e. the combined distribution of all the elements was approximated by the product of individual element distributions [27]. Secondly, the distribution of each individual parameter/state was approximated by the first two moments (mean and variance) known as Laplace approximation [27]. The mean-field approximation and the Laplace approximation allow for an iterative update of the parameters and the states by applying variational calculus. The logarithm of $p(y_t|M)$ is known as 'free energy' $\mathcal{F}(\theta, y_t)$, a term borrowed from statistical physics [25]. The free energy was maximised, and, among other criteria (normalised root mean square error and the stability of the immune response, both of which are discussed in the next section), defined the goodness of fit.

This Bayesian approach not only provides the most probable values of the parameters but also accounts for the uncertainties in the parameters. The prior information regarding the parameters is also taken into account. Such information on possible parameter values was not available to us, and therefore the mean values of the parameter priors were set to zero. To allow the algorithm to search in a relatively wide region for the optimal parameters, all variances were set to be 10^4, i.e. priors with wide distributions were considered. Both noise precisions, which are inversely proportional to noise intensities, were modelled by a gamma distribution with two hyperparameters (shape η_a, ε_a and rate η_b, ε_b). Weakly

informative Jeffreys priors, as described in [28], were chosen for the precisions of the noise, with both shape and rate parameters set to 1. The initial conditions were all modelled as Gaussian distributions. The prior means of the initial conditions were defined from the measurement time series, and the prior variances were set to 10^4.

3.3. Model selection criteria

The following four criteria were applied to identify the best fitting model.

1. *The free energy* $\mathcal{F}$ has been maximised by tuning system parameters in an iterative manner for each model. Note that decision making based on the comparison of free energy of any two models with different orders could be problematic due to the heavy penalisation of the model complexity embedded in the variational Bayesian method as explained in [27]. Increasing the order of the system by one would not only increase the degree of freedom in the parameter space, but also increase the dimension of the system states. This leads to a dramatic decrease in the free energy, which could be an order (or several orders) greater than the free energy difference between models of the same order. Therefore, the free energy criteria was only used to compare the models of the same order. For models with different orders, criterion 2, as below, was utilised.
2. *Normalised Root Mean Squared Error (NRMSE)* was used to compare the models with different orders for each individual time series. Inferred parameters θ_i were applied back to the system equation to generate time series without stochastic terms, i.e. deterministic solution. Note that because parameters were identified in the form of normal distributions, the most probable (mean) value of parameters were plugged into the system equation. Root Mean Squared Error (*RMSE*) between the measurement MFI time series y_t and the inferred deterministic time series $\hat{y}_t$ can be calculated as follows:

$$RMSE = \sqrt{\frac{\sum_{t=1}^{n}(\hat{y}_t - y_t)^2}{n}} \tag{3}$$

   NRMSE accounts for the different heights of the peaks for each DSA time series and is found by dividing the *RMSE* by the maximal MFI value for a given DSA time series. The model with the lowest value of *NRMSE* describes the data most accurately. For the model to be deemed satisfactory, *NRMSE* should not exceed the value of 0.15 (or 15 %) as it is known that the inter-assay coefficient of variability for DSA measurements is around 10–30% [29].
3. *Generic form*. As the entire aim was to find a model capable of capturing the common patterns in all time series, a model that could only describe some of the DSA time series was disregarded.
4. *System stability*. The model has to have a unique stable steady state, which implies that the system's response decays with time. This has been checked via calculations of the real parts of corresponding eigenvalues which have to be negative for stability. Note, even though the steady state of the immune homoeostasis was disturbed by transplantation, the antibody levels settled rapidly to a new steady state except for the extreme cases (example case 69 HLA-DR53 in Fig. 2), but consideration of such cases is out of the scope of this work.

3.4. Statistical analysis

Statistical analysis of model parameters was performed using the Wilcoxon rank sum test. The null hypothesis of no difference between the groups of interest was tested at the 5% significance level, and the results are presented as p-values. Statistical analysis of the differences in *NRMSE* between two models was performed using the one sample t-test, which assesses the normality of data with zero mean and unknown variance at the 5% significance level. The result is presented as p-values.

4. Results and discussions

4.1. Model selection

4.1.1. Comparison of linear models of different orders

Linear models with different system orders are considered first. Eq. (1) in Section 3.1.2 transforms into a linear differential equation when $f_{i+1}(x_t)$ are constants, with constant parameters θ_i $(i = 0, 1, \ldots, n-1)$, where $f_n(x_t) = \theta_n, \ldots, f_2(x_t) = \theta_2, f_1(x_t) = \theta_1$. $f_0(x_t)$ is defined as $-\theta_0$ for convenience.

A first order linear model was considered first, and it did not show good performance. Then linear models with higher system orders were investigated. In this section, we present the results of system and parameter identification by comparing solutions for linear first, second and third order dynamic equations only:

$$\text{Model 1 } (M_1): \quad \frac{dx_t}{dt} + \theta_1 x_t - \theta_0 = 0 \tag{4}$$

$$\text{Model 2 } (M_2): \quad \frac{d^2x_t}{dt^2} + \theta_2\frac{dx_t}{dt} + \theta_1 x_t - \theta_0 = 0 \tag{5}$$

$$\text{Model 3 } (M_3): \quad \frac{d^3x_t}{dt^3} + \theta_3\frac{d^2x_t}{dt^2} + \theta_2\frac{dx_t}{dt} + \theta_1 x_t - \theta_0 = 0 \tag{6}$$

Note if the third order equation had not been successful, the procedure would have continued to account for nonlinearities (presented in Section 4.1.2) first and then increase the order of the system until a suitable solution is found.

Initially not only the measurement noise ε_t (as in Eq. (2)) but also the system noise η_t (as in Eq. (1)) was included in the models. It was found that for all DSA time series, models without system noise have larger free energy compared with the counterpart mathematical representations containing both types of stochasticity. The benefit – improved fitting – obtained by using the more complex model with system noise does not exceed the penalty introduced by adding two degrees of freedom in the parameter space. Therefore, we excluded the system noise from the models and this is reflected on the zero right hand side of the Eqs. (4)–(6).

Typical fittings for four DSA time series, one from the no-AMR group and the other three from the AMR group, by the three suggested models (4)–(6) are shown in Fig. 3. The results for models M_1 – M_3 in Fig. 3(a) and (c) show a winning model candidate M_3. Even though (a) is from a patient in the no-AMR group and (c) is from a patient in the AMR group, both time series show oscillations after day 30. M_1 failed to describe the dynamics of both time series as indicated by large *NRMSE* values in Table 1: $NRMSE = 0.272$ and $NRMSE = 0.090$. M_2 successfully described the initial falls for both time series, but failed to capture the oscillations in DSA after day 30, which is also confirmed by the large *NRMSE* value of 0.053 and 0.096 (Table 1). M_3 captured successfully both the falling part and the later trend with smaller *NRMSE* values of 0.014 and 0.053. Fig. 3(b) exhibits different dynamics with a cluster of data around day 20. This is a common feature observed in the majority of time series in both AMR and no-AMR groups, and requires special attention. The temporary stall of falling could not be expressed by using M_1 or M_2; however, M_3 successfully depicted the sudden changes in falling as shown in the magnified box 1

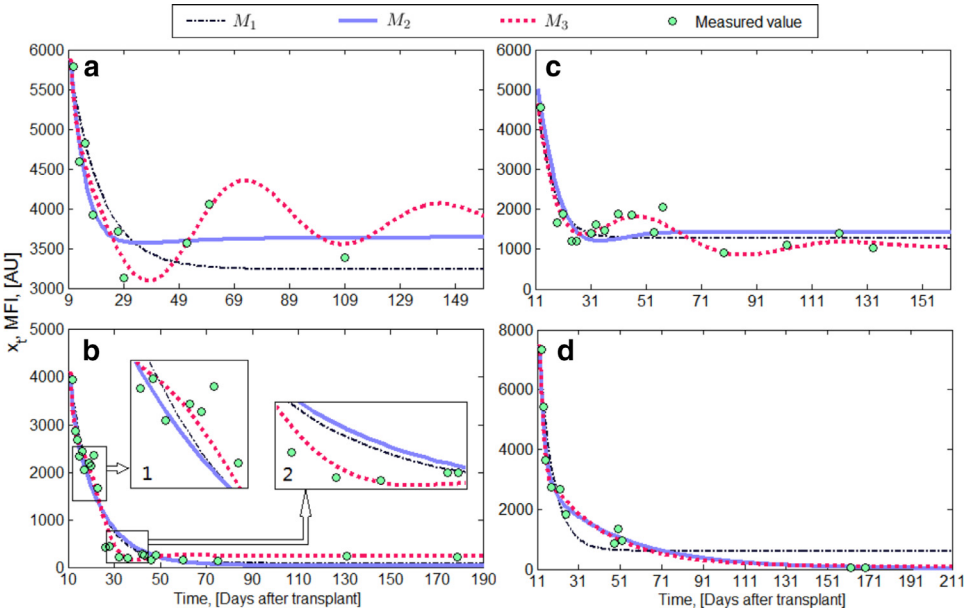

Fig. 3. Typical fitting results compared among the three models M_1 – M_3 for (a) HLA-B60 (case 52) for a patient from the no-AMR group; (b) HLA-DRB3*01 for a patient (case 14) from the AMR group; (c) HLA-A32 for a patient (case 16) from the AMR group; (d) HLA-A2 for a patient (case 17) from the AMR group. The measured values are indicated by circles.

Table 1
Summary of the *NRMSE* values for 3 models corresponding to the four example datasets in Fig. 3.

	NRMSE		
	M_1	M_2	M_3
(*a*)	0.272	0.053	0.014
(*b*)	0.083	0.085	0.013
(*c*)	0.090	0.096	0.053
(*d*)	0.088	0.071	0.073

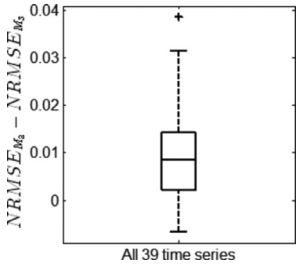

Fig. 4. Boxplot of the difference between the *NRMSE* of M_2 and *NRMSE* of M_3.

in Fig. 3(b). Further, the fittings by M_1 and M_2 were almost indistinguishable after day 70, and both models underestimated the settling level of DSAs. The fitting by M_3 otherwise correctly estimated the settling level and gave a better description of another clustered region around day 30 (see magnified box 2 in Fig. 3(b)). Thus, M_1 and M_2 were ruled out based on their incapability of describing the important features, and the higher order model M_3 was chosen.

The same approach was applied to all the other DSA time series. In 32 out of 39 cases, the *NRMSE* value of M_3 was the smallest among the three models. In the other 7 cases, the *NRMSE* value of M_2 was comparable with the *NRMSE* value of M_3. An example is shown in Fig. 3(d) where the fittings by M_2 and M_3 were indistinguishable from each other, with *NRMSE* values given in Table 1. To compare the *NRMSE* values between M_2 and M_3 across all 39 cases, the *NRMSE* value of M_3 was subtracted from the *NRMSE* of M_2, and the differences for all time series are shown in the boxplot Fig. 4. The differences in *NRMSE* between the two models were tested by the one-sample *t*-test at the significance level of 0.001, and the mean value was found to be significantly larger than zero. Therefore, M_3 was selected as the best model across the cohort with the dynamic equation in the form (6). Note that the $NRMSE_{M_2} - NRMSE_{M_3}$ values for the seven cases with very close *NRMSE* values, mentioned above, are located around the zero value in Fig. 4.

4.1.2. Nonlinear versus linear

Nonlinearity was introduced into the second order model in the form of polynomial nonlinear coefficients $f_1(x_t)$ or $f_2(x_t)$ in Eq. (1) using the approach of [23,30,31]. It was acknowledged that a linear description is preferable over nonlinear if this does not increase the number of unknown parameters dramatically. Consequently, the maximal number of unknown parameters in the second order nonlinear model was kept comparable with the number of parameters of the third order linear equation, i.e. no more than 4. Under this condition, two nonlinear models were considered: model NM_1 with nonlinearity in the damping term ($f_1(x_t) = k_1x_t + \theta_1,\ f_2(x_t) = \theta_2$) and model NM_2 with nonlinearity in the x_t term ($f_1(x_t) = \theta_1,\ f_2(x_t) = k_2x_t + \theta_2$). The corresponding system equations are as follows:

$$NM_1:\ \frac{d^2x_t}{dt^2} + \theta_2\frac{dx_t}{dt} + (k_1x_t + \theta_1)x_t - \theta_0 = 0 \tag{7}$$

$$NM_2:\ \frac{d^2x_t}{dt^2} + (k_2x_t + \theta_2)\frac{dx_t}{dt} + \theta_1x_t - \theta_0 = 0 \tag{8}$$

An example of the fittings of the time series from Fig. 3(c) by nonlinear models NM_1 and NM_2 is shown in Fig. 5. From Fig. 5, neither NM_1 nor NM_2 captured the dynamic features of the time series. The *NRMSE* criterion was applied here for models of different order: both *NRMSE* values (0.080 for NM_1 and 0.067 for NM_2) are larger than 0.053 for M_3. Additionally it is clear that the fitting

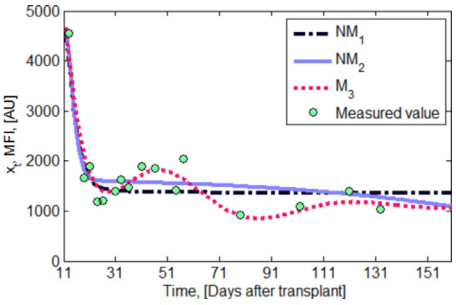

Fig. 5. Fitting results compared between the two nonlinear models NM_1 and NM_2 and the linear model $M3$ for the time series shown in Fig. 3(c). The measured values are indicated by circles.

by NM_2 leads to an unstable solution. Therefore, linear model M_3 (Eq. 6) outperformed both NM_1 and NM_2, and was chosen as the final model. This example is a typical (representative) fitting for all the other time series in the cohort.

4.2. Analysis of the inferred parameters

The inferred parameters (θ_0, θ_1, θ_2 and θ_3) of the selected model M_3 have been compared between the two groups (AMR and no-AMR) for meaningful differences. The results are presented in Fig. 6(a)–(d) in the form of boxplots. For all four parameters, the ranges of the parameter values are much wider in the AMR group compared with the no-AMR group, indicating more diverse dynamic behaviour of DSAs in the AMR group. The Wilcoxon rank sum test showed statistically significant differences in the median values between the AMR and the no-AMR group for all four parameters, which confirmed the results of our preliminary study [23] with fewer cases.

Even though the values of the parameters do not have direct clinical interpretations, which is one of the main drawbacks of data-driven modelling in biomedical research, a certain combination of the parameters indicates important features of the system under investigation. The ratio θ_0/θ_1 from Eq. (6) defines the settling level of DSA, which is of clinical interest. Kidney transplantation constitutes a major disturbance in the immune system, and the system should settle down to a new homoeostatic equilibrium after the transient response to the transplanted organ. A successful transplantation is usually characterised by a new stable steady state with low DSA levels (ideally zero, or below the limit of detection of the assay). From the comparison between the AMR and no-AMR groups, the majority of the settling MFI values in both groups are less than 1000 AU, indicating low DSA settling levels. The highest settling level in the no-AMR group is 3862 AU, compared with the level of 5783 AU in the AMR group. The lowest settling level in the no-AMR group is 22 AU, compared with the level of 27 AU in the AMR group. There is no significant difference in the median value of θ_0/θ_1 between the groups with a p-value of 0.5 (300 AU in the no-AMR group, 425 AU in the AMR group), which means that a DSA time series from the AMR group does not necessarily have a higher settling level. However, significant difference in θ_0 and θ_1 separately between the groups shown in Fig. 6 implies that the dynamic behaviour of DSAs in the AMR group might be controlled by more complex and diverse underlying mechanisms.

Such detailed analysis of the parameters of the models developed allows for enhanced understanding of the clinical characteristics which are most important for successful outcome in this high risk form of transplantation. Our findings may facilitate the formation of an accurate pre-transplant risk profile which predicts AMR and allows the clinician to intervene at a much earlier stage. Given that AMR in the early post-transplant period has been shown to lead to worse long-term graft outcome any strategy to prevent early AMR will be of great benefit to the patients [15].

Noise accounts for both measurement error due to inaccuracy in the MFI readings, and the perpetual actions of many unaccounted for factors that influence the evolution of the system. The noise intensities I_ε were compared between the no-AMR and AMR groups. Our preliminary study [23] showed a smaller and more compact range of the noise intensities from the no-AMR group with 9 time series compared with the AMR group with 12 time series (shown in Fig. 5 of [23]). Limited by the numbers of cases available then, the Wilcoxon rank sum test showed no significant difference in the median value between groups with a p-value of 0.08. This study, on a larger cohort with almost twice as many time series, confirmed the previous observation with a smaller p-value of 0.01, indicating a significant difference in the median values of the noise intensity between groups.

The square root of the noise intensity $\sqrt{I_\varepsilon}$, which is an absolute error value, shares the same unit as the MFI level. In the no-AMR group with an average MFI peak height of 5716 AU, the median and range (in brackets) for $\sqrt{I_\varepsilon}$ were 159 (5–353) AU. In the AMR group with an average MFI peak height of 8502 AU, the median and range (in brackets) for $\sqrt{I_\varepsilon}$ were 253 (34–1425) AU. A smaller noise intensity and more compact range of values across the

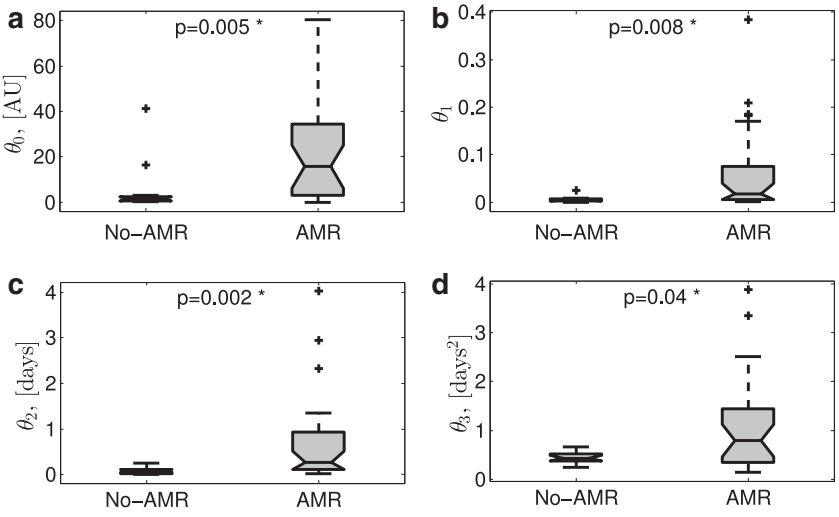

Fig. 6. Boxplot for the inferred parameters θ_0, θ_1, θ_2, θ_3.

no-AMR group is noticeable. Even though the assay used to measure the DSA level in both groups was the same, the relationship between MFI measurement and the antibody level deviates from linearity as the antibody level approaches 10,000 AU. The higher antibody peak values in the AMR group can therefore introduce an additional source of measurement error compared with the no-AMR group, explaining the wider range and greater magnitude of noise intensity seen in the AMR group. Another explanation could be a different level of model imperfection between the two groups. The higher level of noise in the AMR group could be caused by more and/or stronger factors unaccounted for by M_3. Also it is worth noticing that the priors for the noise intensity applied in the inference method are chosen to be weakly informative. A more informative prior may limit the flexibility of the model, but a carefully chosen informative prior could improve the estimation of deterministic parameters and parameters related to noise description. The choice of the priors is not straightforward, and an appropriate methodology is under development.

In single antigen bead measurements, another measure, termed *inter-assay coefficient of variability (CV)* is often used to indicate the measurement uncertainty. It is defined as the ratio of the standard deviation and the mean value of several measurements using separate assays. In [32], the inter-assay CV was larger than 20% when the measurements from seven different labs were compared. In our model, considering the median value of $\sqrt{I_\varepsilon}$ and the median value of MFI measurements, the median CV is 13% and 14% for the no-AMR and AMR group respectively, which is less than 20% given in [32].

4.3. Eigenvalues

The evolution equation Eq. (6) can be transformed into the third order linear state space model of the form

$$\begin{pmatrix} \dot{x}_t \\ \ddot{x}_t \\ \dddot{x}_t \end{pmatrix} = \begin{pmatrix} 0 & 1 & 0 \\ 0 & 0 & 1 \\ -\theta_1 & -\theta_2 & -\theta_3 \end{pmatrix} \begin{pmatrix} x_t \\ \dot{x}_t \\ \ddot{x}_t \end{pmatrix} + \begin{pmatrix} 0 \\ 0 \\ \theta_0 \end{pmatrix} \tag{9}$$

The solution of Eq. (9) is defined by the eigenvalues λ_1, λ_2, λ_3 of the 3×3 matrix, the corresponding eigenvectors and three initial conditions. The sum of the eigenvalues defines the divergence of the vector field (phase volume $V(t)$) in the state space [33]:

$$V(t) = V_0 e^{(\lambda_1+\lambda_2+\lambda_3)t} = V_0 e^{Rt}, \tag{10}$$

where R can be interpreted as the dissipation rate of DSAs. For all the time series in the cohort, the dissipation rate is less than zero, which means that the phase volume shrinks.

The eigenvalues for every DSA time series were calculated using the inferred parameters θ_1, θ_2 and θ_3. Each DSA time series in the cohort is characterised by three eigenvalues, one of which is real, λ_1, and two of which are complex conjugate, $\lambda_{2,3} = \lambda_r \pm i\lambda_i$. All eigenvalues λ_1 and the real parts of λ_2 and λ_3 were negative, confirming that the system generates stable solutions for each DSA type, which satisfies criterion 4 in Section 3.3. The system dynamics for each DSA demonstrate a decay with some oscillations, the frequency of which is determined by λ_i. The dissipation rate is determined by the real parts of the eigenvalues: $R = \lambda_1 + 2\lambda_r$. The characteristic dissipation rate R takes into account the overall decay along the path from the peak value down to the steady state. The steady state of the system is a fixed point, which serves as an attractor. To visualise the dynamics of DSAs, phase portraits have been plotted for an AMR case (Fig. 7(a)), and a no-AMR case (Fig. 7(b)). The trajectories start from the inferred initial states and evolute to the fixed points in a spiral manner in the phase space. It can be seen that the dissipation rate in the AMR group (Fig. 7(a), $R_{(a)} = -0.81$ days^{-1}) is faster than in the no-AMR group (Fig. 7(b), $R_{(b)} = -0.27$ days^{-1}).

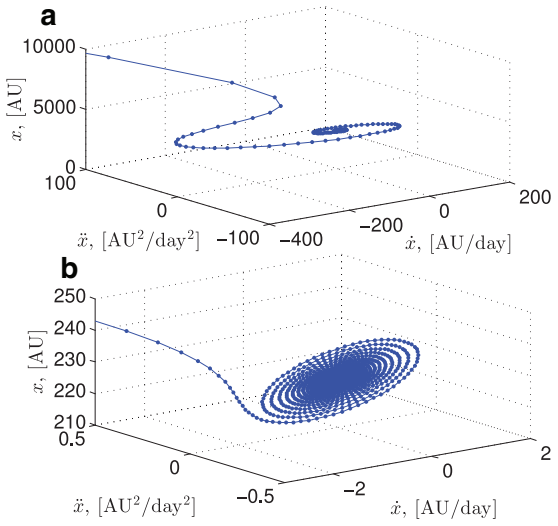

Fig. 7. Phase portraits of the three dimensional system for two DSA time series, (a) from a patient in the AMR group and (b) from a patient in the no-AMR group. The time difference between two consecutive markers is one day.

The dissipation rates and frequencies of oscillations were compared between the AMR and no-AMR groups for 39 time series. In the no-AMR group, the median and range (in brackets) for R were -0.42 ($-0.66-$: 0.25) days^{-1}. In the AMR group, the median and range (in brackets) for R were -0.79 ($-3.88-$: 0.15) days^{-1}. The comparison of the dissipation rates R between the groups for all the time series confirmed a significantly faster dissipation rate of DSAs in the AMR group than in the no-AMR group with a p-value of 0.04.

The imaginary parts of the eigenvalues between AMR and no-AMR groups also showed significant differences with a p-value of 0.03. In the no-AMR group, the median and range (in brackets) for λ_i were 0.20 (0.01 : 0.34) days^{-1}. In the AMR group, the median and range (in brackets) for λ_i were 0.28 (0.05 : 0.80) days^{-1}. The larger values of the imaginary parts in the AMR group represent a higher frequency of oscillation, which indicates a stronger regulation during the transient antibody response for the patients in the AMR group. One hypothesis of this regulation is the possible production of a secondary antibody (such as anti-idiotype) which targets the dramatically increased DSA, resulting in a battling force between the DSA production and secondary antibody production [19].

Note that the previous study by Higgins et al. [2] investigated the change in absolute MFI values and in the mean percentage falls in the AMR and no-AMR groups, and suggested that the falls were greater in the AMR group compared with the no-AMR group. Our results show that not only is the difference in the MFI level between peak and steady state different between the two groups, but the rate of change of the fall is faster in the AMR group, also implying a stronger regulation mechanism in this group.

5. Conclusions

With a unique dataset of DSA time series available, a mathematical model in the form of differential equations has been developed for the first time to describe the dynamic of the 'falls' in DSAs for patients with and without AMR episodes. The third order linear model was selected as it successfully captured the common features of the falling dynamics in DSAs during the early post-transplant stage in the AMR and no-AMR groups. The model is proved useful in classification between two clinically different groups. Even though the settling level of DSAs, which can be ob-

served from the clinical data, showed no difference between the AMR and the no-AMR groups, all the parameters of the model (both deterministic and stochastic) were found to be significantly different between the two groups. This approach is found to be useful in capturing properties of antibody evolution from their peak concentration to final settling level and showed that the dynamic responses are different in AMR and no-AMR groups. A higher frequency of oscillations and a faster antibody dissipation rate for the AMR group had been observed from the phase portrait depicting the trajectories of the system states, and a further test confirmed significant differences between the groups.

The findings have important implications for the development of laboratory assays that might define the nature of the mechanisms responsible for the falls in DSA levels post-transplant, since a fuller understanding of these mechanisms might allow for pre-transplant manipulation of DSA levels and improved clinical outcomes. This is particularly important with respect to the oscillating nature of DSA levels, which may reflect a system slowly reaching homeostasis, and may be reflected in laboratory measurements.

Further work might also include modelling in relation to more detailed characteristics of the antibodies. For example, we have already shown that the subclasses of IgG are associated with clinical outcomes, so that measuring the levels of these subclasses at more time points might be valuable [34]. The clinical outcome measures might also be extended. Since acute AMR is often treatable and is not always associated with a poor clinical outcome (especially when the settling level of DSA is very low), longer term graft survival could also be considered as an important outcome level. The day to day renal function does not always follow DSA levels [8] and our understanding of how a graft responds to DSA levels and how AMR evolves is limited.

This study comprises a pilot research on data-driven model development for early post-transplant antibody dynamics, focusing on one of the typical patterns of a rapid fall following a rapid rise in DSA after kidney transplantation. Future work will involve classifying and modelling the other patterns of the post-transplant DSA dynamics that have been described in section 2; a universal model that is capable of describing different dynamics in DSAs is under development.

Details on the data used for analysis are available from the University of Warwick institutional repository at http://wrap.warwick.ac.uk/78888/.

Acknowledgment

This work has been supported by EPSRC UK (EP/K02504X/1).

References

[1] L.D. Cornell, R.N. Smith, L.B. Colvin, Kidney transplantation: mechanisms of rejection and acceptance, Annu. Rev. Pathol. Mech. Dis. 3 (2) (2008) 189–220.
[2] R. Higgins, D. Lowe, M. Hathaway, H. Kashi, L.C. Tan, C. Imray, S. Fletcher, K. Chen, N. Krishnan, R. Hamer, Others, rises and falls in donor-specific and third-party HLA antibody levels after antibody incompatible transplantation, Transplantation 87 (6) (2009) 882–888.
[3] S.B. Moore, S. Sterioff, A.M. Pierides, S.K. Watts, C.M. Ruud, Transfusion-induced alloimmunization in patients awaiting renal allografts, Vox Sang. 47 (5) (1984) 354–361.
[4] M. Cascalho, J.L. Platt, Basic mechanisms of humoral rejection, Pediatr. Transplant. 9 (1) (2005) 9–16.
[5] J. Gloor, M.D. Stegall, Sensitized renal transplant recipients: current protocols and future directions, Nat. Rev. Nephrol. 6 (5) (2010) 297–306.
[6] R.M. Higgins, D.J. Bevan, B.S. Carey, C.K. Lea, M. Fallon, R. Bühler, R.W. Vaughan, P.J. O'Donnell, S.A. Snowden, M. Bewick, B.M. Hendry, Prevention of hyperacute rejection by removal of antibodies to HLA immediately before renal transplantation, Lancet 384 (1208) (1996) 1208–1211.
[7] R. Higgins, D. Lowe, M. Hathaway, F.T. Lam, H. Kashi, L.C. Tan, C. Imray, S. Fletcher, K. Chen, N. Krishnan, R. Hamer, D. Zehnder, D. Briggs, Double filtration plasmapheresis in antibody-incompatible kidney transplantation, Ther. Apher. Dial. 14 (4) (2010) 392–399.
[8] R. Higgins, M. Hathaway, D. Lowe, H. Kashi, L.C. Tan, C. Imray, S. Fletcher, D. Zehnder, K. Chen, N. Krishnan, Blood levels of donor-specific human leukocyte antigen antibodies after renal transplantation: resolution of rejection in the presence of circulating donor-specific antibody, Transplantation 84 (7) (2007) 876–884.
[9] J. Sellarés, D.G. De Freitas, M. Mengel, J. Reeve, G. Einecke, B. Sis, L.G. Hidalgo, K. Famulski, A. Matas, P.F. Halloran, Understanding the causes of kidney transplant failure: The dominant role of antibody-mediated rejection and nonadherence, Am. J. Transplant. 12 (2) (2012) 388–399.
[10] P.I. Terasaki, J. Cai, Human leukocyte antigen antibodies and chronic rejection: from association to causation, Transplantation 86 (3) (2008) 377–383.
[11] A.A. Zachary, M.S. Leffell, Detecting and monitoring human leukocyte antigen specific antibodies, Hum. Immunol. 69 (10) (2008) 591–604.
[12] C. Puttarajappa, R. Shapiro, H.P. Tan, Antibody-mediated rejection in kidney transplantation: a review, J. Transplant. 2012 (193724) (2012) 1–9.
[13] J.E. Worthington, A.M. Ewen, L.J.M. William, M.L. Picton, S. Martin, Association between c4d staining in renal transplant biopsies, production of donor-specific HLA antibodies, and graft outcome, Transplantation 83 (4) (2007) 398–403.
[14] P.I. Terasaki, M. Ozawa, Predicting kidney graft failure by HLA antibodies: a prospective trial, Am. J. Transplant. 4 (3) (2004) 438–443.
[15] R. Higgins, D. Lowe, M. Hathaway, C. Williams, F.T. Lam, H. Kashi, L.C. Tan, C. Imray, S. Fletcher, K. Chen, N. Krishnan, R. Hamer, S. Daga, M. Edey, D. Zehnder, D. Briggs, Human leukocyte antigen antibody-incompatible renal transplantation: excellent medium-term outcomes with negative cytotoxic crossmatch, Transplantation 92 (8) (2011) 900–906.
[16] M.R. Clatworthy, Targeting b cells and antibody in transplantation, Am. J. Transplant. 11 (7) (2011) 1359–1367.
[17] A. Morell, W.D. Terry, T.A. Waldmann, Metabolic properties of IgG subclasses in man, J. Clin. Investig. 49 (4) (1970) 673–680.
[18] D. Lowe, S. Shabir, J. Buckels, P. Muiesan, G. Hayden, A. Holt, A. Hamsho, K. Skordilis, G. Lipkin, R. Borrows, D. Briggs, HLA incompatible combined liver-kidney transplantation: dynamics of antibody modulation revealed by a novel approach to HLA antibody characterisation, Transpl. Immunol. 30 (1) (2014) 30–33.
[19] E. Reed, M. Hardy, A. Benvenisty, C. Lattes, J. Brensilver, R. McCabe, K. Reemstma, D.W. King, N. Suciu-Foca, Effect of antiidiotypic antibodies to HLA on graft survival in renal-allograft recipients, N. Engl. J. Med. 316 (23) (1987) 1450–1455.
[20] P.S. de Souza, E. David-Neto, N. Panajotopolous, F. Agena, H. Rodrigues, C. Ronda, D.R. David, J. Kalil, W.C. Nahas, M.C.R. de Castro, Dynamics of anti-human leukocyte antigen antibodies after renal transplantation and their impact on graft outcome, Clin. Transplant. 28 (11) (2014) 1234–1243.
[21] O. Thaunat, W. Hanf, V. Dubois, B. McGregor, G. Perrat, C. Chauvet, J.-L. Touraine, E. Morelon, Chronic humoral rejection mediated by anti-HLA-DP alloantibodies: insights into the role of epitope sharing in donor-specific and non-donor specific alloantibodies generation, Transpl. Immunol. 20 (4) (2009) 209–211.
[22] S.M. Dunn, A. Constantinides, P.V. Moghe, Dynamic systems : ordinary differential equations, in: Numerical Methods in Biomedical Engineering, Academic Press Series in Biomedical Engineering, 2007, pp. 209–287. Chapter 7.
[23] Y. Zhang, D. Lowe, D. Briggs, R. Higgins, N. Khovanova, Novel data-driven stochastic model for antibody dynamics in kidney transplantation, in: Proceedings of the Ninth IFAC Symposium on Biological and Medical Systems, BMS 2015, 48, 2015, pp. 249–254. (20), FAC-PapersOnLine.
[24] MATLAB, Version 8.2.0.701, The MathWorks Inc., vol. 2013, 2013.
[25] J. Daunizeau, K.J. Friston, S.J. Kiebel, Variational Bayesian identification and prediction of stochastic nonlinear dynamic causal models, Phys. D Nonlinear Phenom. 238 (21) (2009) 2089–2118.
[26] SPM, in: The toolbox is an extention of SPM package developed at UCL, UK, 2009. www.fil.ion.ucl.ac.uk/spm.
[27] M.J. Beal, Variational Algorithms for Approximate Bayesian Inference (Ph.D. thesis), The Gatsby Computational Neuroscience Unit, University College London, 2003. pp. 1–281.
[28] A. Gelman, J.B. Carlin, H.S. Stern, D.B. Rubin, Bayesian Data Analysis, 2, Taylor & Francis, 2014.
[29] E.S. Woodle, a.R. Shields, N.S. Ejaz, B. Sadaka, A. Girnita, R.C. Walsh, R.R. Alloway, P. Brailey, M.A. Cardi, B.G.A. Jawdeh, P. Roy-Chaudhury, A. Govil, G. Mogilishetty, Prospective iterative trial of proteasome inhibitor-based desensitization, Am. J. Transplant. 15 (1) (2015) 101–118.
[30] N. Khovanova, Y. Zhang, T.A. Holt, Generalised stochastic model for characterisation of subcutaneous glucose time series, in: Proceedings of the IEEE-EMBS International Conference on Biomedical and Health Informatics (BHI), 2014, pp. 484–487.
[31] Y. Zhang, T.A. Holt, N. Khovanova, A data driven nonlinear stochastic model for blood glucose dynamics, Comput. Methods Progr. Biomed. 125 (2015) 18–25.
[32] E.F. Reed, P. Rao, Z. Zhang, H. Gebel, R.A. Bray, I. Guleria, J. Lunz, T. Mohanakumar, P. Nickerson, a.R. Tambur, A. Zeevi, P.S. Heeger, D. Gjertson, Comprehensive assessment and standardization of solid phase multiplex-bead arrays for the detection of antibodies to HLA, Am. J. Transplant. 13 (7) (2013) 1859–1870.
[33] L. Arnold, Stochastic Differential Equations: Theory and Applications, New York. John Wiley & Sons, 1973.
[34] N. Khovanova, S. Daga, T. Shaikhina, N. Krishnan, J. Jones, D. Zehnder, D. Mitchell, R. Higgins, D. Briggs, D. Lowe, Subclass analysis of donor HLA-specific IgG in antibody-incompatible renal transplantation reveals a significant association of IgG 4 with rejection and graft failure, Transpl. Int. 28 (2015) 1405–1415.